ACS APPLIED MATERIALS & INTERFACES

Research Article

www.acsami.org

Selective Growth of Silver Nanoparticle Arrays on Nanoimprinted Sol–Gel Silica Patterns

Chi-Kai Chiu* and Tzy-Jiun M. Luo

Department of Materials Science and Engineering, NC State University, Raleigh, North Carolina 27695, United States

ABSTRACT: Selective growth of silver nanoparticles on ~100 nm thick silica patterns produced by nanoimprint method has been successfully demonstrated using either (1) thermo-induced reduction or (2) room temperature electroless deposition (ELD) without removing the ~25 nm thick residual layer left by nanoimprint process. This selectivity was achieved by silane additive, (3-mercaptopropyl)-trimethoxysilane (3-MTS), which was added to the silica matrix to control nucleation and growth of silver. The presence of silver nanoparticles was confirmed by EDX and UV–vis spectrum, and the density, distribution, and size of silver particles were examined by atomic force microscopy (AFM) and scanning electron microscopy (SEM). Silica film heat-treated between 400 and 600 °C resulted in silver particles of 100–120 nm diameter with a linear density of 2.63–3.36 μm^{-1}, while the film treated by room temperature ELD produced silver particles of 67 nm diameter with a linear density of 5.65 μm^{-1}. The selective growth ratio based on particle density on pattern area versus residual layer is 12.92 and 20.31 for high- and room-temperature processes, respectively, whereas the samples without 3-MTS shows low selective growth ratio of 1.22 and 1.04. These results prove that both approaches are fast and effective, suggesting their potential to produce other type of nanoparticle arrays directly on nanoimprinted patterns.

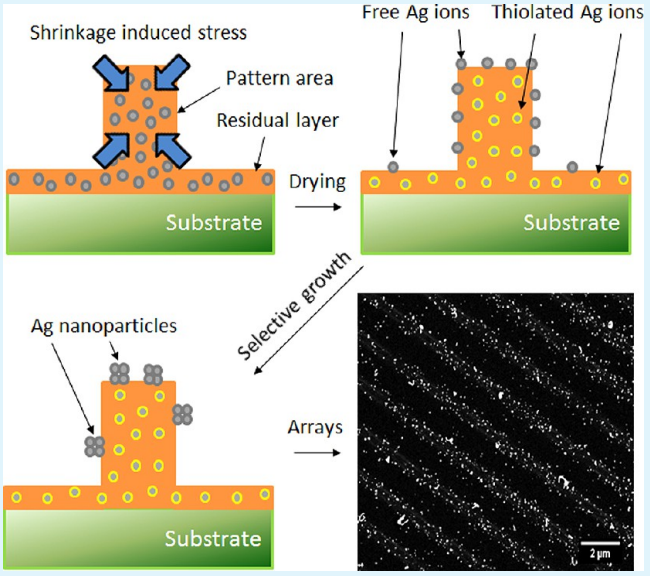

KEYWORDS: *nanoparticle array, nanoimprint, residual layer, pattern, sol–gel*

1. INTRODUCTION

To fully utilize the properties of nanoparticles in applications such as optics,[1,2] microelectronics,[3,4] and biosensors,[5,6] nanoparticles are often required to be constructed into patterned arrays.[7] For example, an array of metallic nanoparticles is able to exceed the diffraction limit and interact with light at subwavelength region, making it possible to create optoelectronics and light emission devices.[8,9] Also, metal nanoparticle arrays have been shown with better sensitivity as a biosensor for detecting biological molecules of low binding affinity.[10] Currently, all techniques fall within two approaches. The first approach, known as the top-down method, utilizes lithography methods to create patterns followed by deposition of nanoparticles. For example, electron beam lithography has been utilized to create arrays of patterns about the size of 100 nm to deposit citrate-functionalized nanoparticles.[11] Although accurate, this technique heavily relies on the resolution of the irradiation source, and is often slow and costly. To improve it, Kuznetsov et al. developed a fast and low-cost method that combines nanosphere lithography and laser-induced pattern transfer.[12] However, to produce large coverage of nanoparticles without defects remains a challenge. Second approach, the bottom-up method, utilizes the different interactions between patterned surface and nanoparticles to guide the self-assembly of nanoparticles. Several groups have successfully created close-packed and regular arrays of nanoparticles that were self-assembled using micelles of block copolymer via dip coating or spin coating technique.[13,14] Self-assembly is inexpensive and highly scalable but the resulting structures are often filled with defects. To achieve high quality patterns, researchers now are focusing on combining nanoimprint lithography and self-assembly of nanoparticle to fabricate patterned arrays. For example, arrays of nanoparticle pattern have been demonstrated using nanoimprinted layer and self-assembly of nanoparticle.[15,16] Using this approach, various nanoscale features can be produced by carefully controlled nanoimprint process followed by self-assembly.[17,18] These methods are accurate, fast, and cost-effective, as the stamp can be reused. However, the nanoimprint method always leaves an undesired residual layer that lowers the selectivity of self-assembly.[19,20] This

Received: December 7, 2012
Accepted: June 3, 2013
Published: June 3, 2013

residual layer is usually removed using either solvent etching or reactive ion etching such as oxygen plasma or reactive ion beam. However, those processes may damage organic layers and introduce defects.[21] Besides, the roll-to-roll nanoimprint process is incompatible with the vacuum system of the plasma etching process. In the present study, a technique sensitive to the film thickness has been developed to selectively grow nanoparticle arrays on nanoimprinted patterns regardless of the presence of residual layer.

Although the controlled growth of nanoparticles commonly involves well-defined 2D or 3D templates,[22−24] selective growth of nanoparticles via film thickness is a simple and fast alternative approach. We have reported that metastable silver nanoparticles and silver chloride nanocrystals remain mobile inside the nanopores of sol−gel film that contains low molecular weight polyethylene glycol (PEG).[25,26] The metastable nanocrystals are able to migrate to the surface when the films are under shrinkage-induced stress and grow into large crystals with their crystal size related to the film thickness. These results suggest the possibility of growing silver nanoparticle arrays on patterned silica films. Here, we present a strategy to selectively grow silver nanoparticles on patterned silica films in the presence of residual layer by controlling the interactions between silver ions and nonporous surfaces using (3-mercaptopropyl)trimethoxysilane (3-MTS) as selectivity enhancement agent. The thiol group of 3-MTS forms covalent bond to gold, silver and platinum atoms and therefore 3-MTS has been utilized to form self-assembled monolayer on gold substrates.[27−29] Similarly, we found 3-MTS also changes the mobility of silver ions in the film, enabling us to control the location, growth density and size of silver nanoparticles using the film thickness. In general, the patterned area is approximate 100 nm thick and the residual layer is ∼25 nm. Two methods have been employed to produce arrays of silver nanoparticles. Method 1 is thermo-induced reduction (Figure 1a), and method 2 is room temperature electroless deposition (Figure 1b). Each method includes two steps: creation of patterned silica film and selective growth of silver nanoparticles. Based on these methods, growth of nanoparticles preferably on the thicker film and thus nanoparticle arrays can be achieved. By combining nanoimprint technique and selective growth of nanoparticles, this fabrication method is simple, effective and could be adapted to pattern nanoparticles of other materials with controllable geometry and dimension.

2. EXPERIMENTAL SECTION

2.1. Preparation of Stock Solutions. TMOS-sol was prepared by mixing 3.6 mL of deionized-water with 15.2 mL of tetramethyl orthosilicate (TMOS, 98%, Sigma-Aldrich). After adding 80 μL of 0.5 N HNO_3, the mixture was transferred into ice bath immediately. During vigorous stirring for 2 min in an ice bath, the solution became clear and uniform. Then, the mixture was sonicated for 20 min. The resulting solution should be colorless and particle-free. PEG-sol was prepared by adding 3.6 mL of DI-water into TMOS-sol and then adding 7.2 mL of poly(ethylene glycol) (PEG, MW = 300 g/mol, Sigma-Aldrich) into the mixture. Methanol was removed from the sol by rotary evaporation (200 mbar reduced pressure, 45 °C) for 35 min to get a viscous PEG-sol.

2.2. Synthesis of Patterned Nanoparticle Arrays. The CD-ROM pattern template was made by cutting a CD-ROM disc (Verbatim brand) into 10 × 10 mm^2 size, and the metal coating was peeled away using scotch tape. The template was sonicated subsequently in isopropyl alcohol (IPA) and methanol solution for 10 min to clean and remove the dye. After sonication, the template was dried by purging air. The glass substrate was made by cutting a glass slide (Fisher brand) into 10 × 10 mm^2 size and then cleaning the cut slide subsequently in IPA and methanol for 10 min sonication. After drying by purging air, the glass substrate was plasma-treated for 2 min immediately before use.

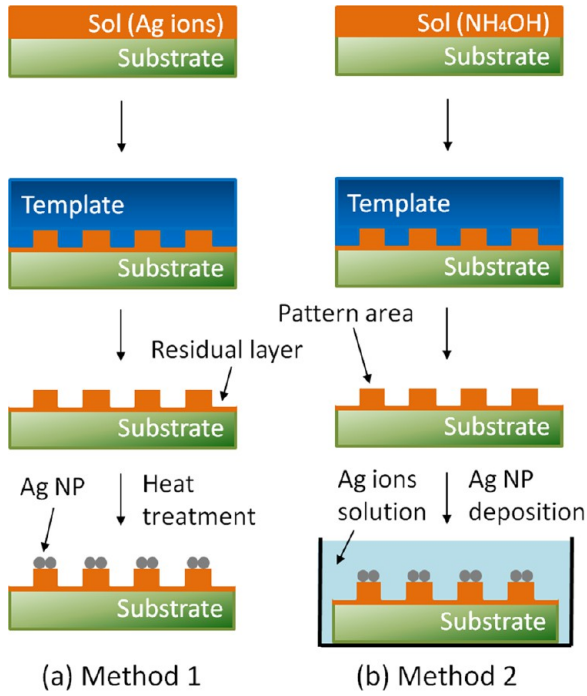

Figure 1. Two methods to create patterned silver nanoparticle arrays. (a) Method 1: A PEG-sol containing silver ion was cast on a glass substrate followed by nanoimprint, drying, and heat treatment. (b) Method 2: A PEG-sol containing ammonium hydroxide was cast on a glass substrate followed by nanoimprint, drying, and room temperature silver deposition in 1 M $AgNO_3$ solution.

Two solutions were employed to create sol−gel patterns and each requires different casting solution. Solution 1: two surface modifying agents used in the first method are (3-mercaptopropyl)-trimethoxysilane (3-MTS, 95%, Gelest) solution (0.1 M in methanol) and polyvinylpyrrolidone (PVP, MW ∼ 36 000 g/mol, Sigma-Aldrich) solution (0.1 M in methanol). Each was used to prepare 3-MTS-treated samples and PVP-treated samples. A volume of 40 μL of modifying agent solution was mixed with 600 μL of 1 M silver nitrate ($AgNO_3$, >99%, Sigma-Aldrich) solution, and the mixture was agitated for 30 s. Then, 200 μL of PEG-sol was added into the mixture and mixed for 30 s. (Note: The PEG-sol should be warmed up to room temperature before using.) Solution 2: 50 μL of 0.14 M ammonia hydroxide and 10 μL of 3-MTS solution were added into 150 μL of methanol. Then, 200 μL of PEG-sol was added into the solution, and the mixture was mixed for 30 s.

After 10 μL of either solution was dropped onto a plasma-treated glass, the glass slide was quickly covered with a CD-ROM template, which was secured using a pressure clamp for 2 h. After removing the template, the sol−gel pattern should be visible on the glass substrate. Then, the pattern was aged in ambient environment for 20 h. Later, the film pattern was treated using one of the following two methods. Method 1: samples produced from Solution 1 was either (a) heat treated at 160 °C with a heating rate of 10 °C/min for 3 h followed by oven cool down to 25 °C, or (b) heat treated at 400 and 600 °C with heating rate of 10 °C/min and heated for 90 min and oven cool down to 25 °C. For Method 2, samples produced from Solution 2 were soaked in 1 M silver nitrate solution for 20 h followed by rinsing with acetone three times and drying by purging air.

2.3. Characterization Methods. Atomic force microscopy (AFM) images were obtained using a Veeco calibrator AFM instrument equipped with phosphorus doped silicon tip. The tapping mode was performed to scan the pattern surface for showing the

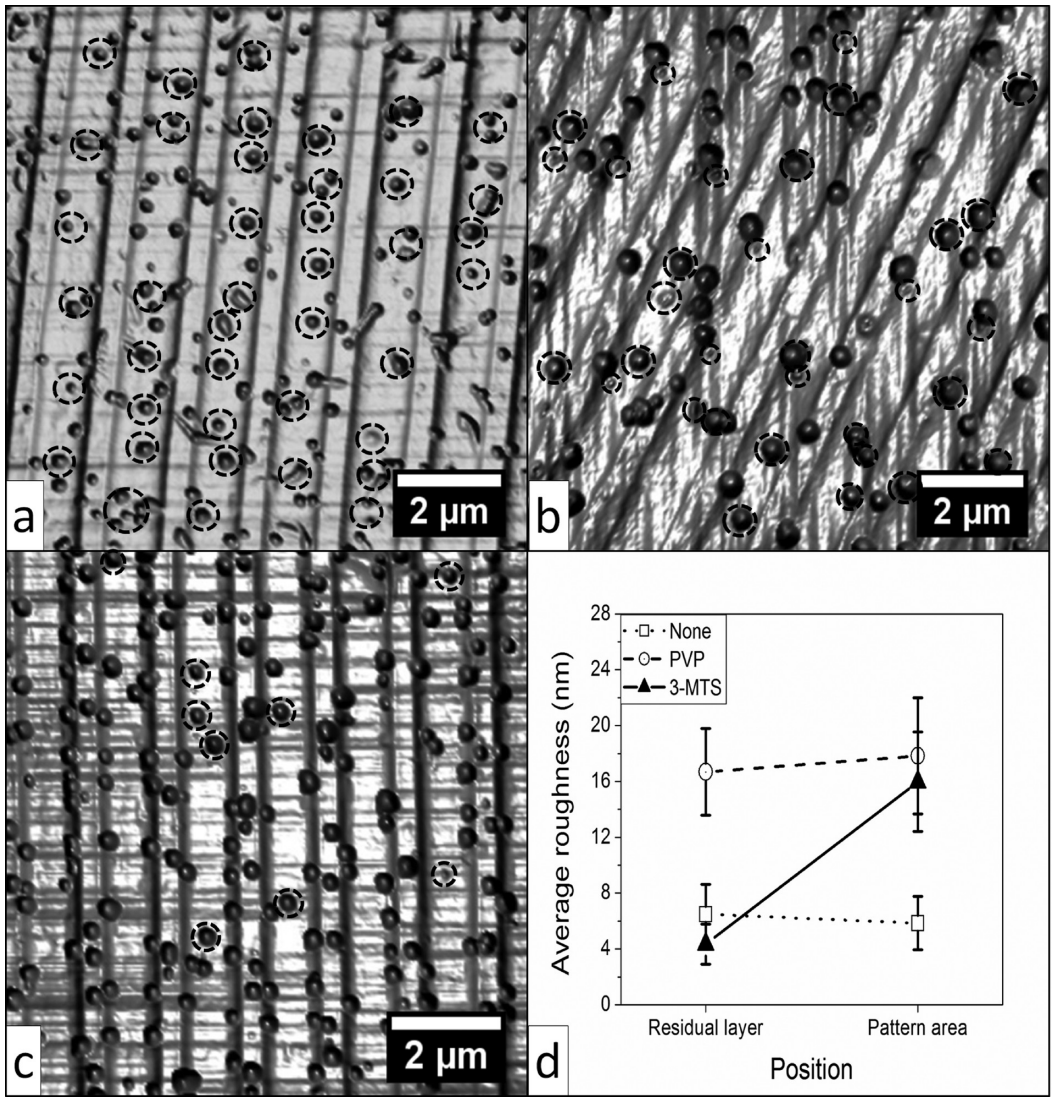

Figure 2. AFM images of patterned silver nanoparticles on sol−gel silica films after heat treatment at 160 °C for 3 h. Each film was created from the same sol−gel solutions labeled as (a) control and with addition of (b) PVP or (c) 3-MTS. Particles on the residual layer are highlighted by dashed circles. The average roughness at different position of each sample is summarized in (d).

particles on the pattern. Scanning electron microscopy (SEM) observation was carried out on a field emission microscope (Hitachi S3200) under an acceleration voltage of 15 kV, and the samples were imaged after sputtering Au−Pd metallic coating. The energy dispersive X-ray spectrometer system attached on the SEM instrument was used to identify the characteristic X-ray emission of the elements at surface to acquire the elemental information. UV−vis spectroscopy was performed on a Varian Cary 100 spectrophotometer equipped with dual beam chamber, where the sol−gel silica patterns on the glass substrate were measured. To ignore the absorption caused by glass substrate, the plain glass substrate was measured at the same time to subtract the substrate effect.

3. RESULTS AND DISCUSSION

AFM images of silver particles on the control, PVP-treated, and 3-MTS-treated samples produced by method 1 after annealing at 160 °C are, respectively, shown in Figure 2a−c. The control sample shows that silver particles with average size of 200 nm randomly distribute on both pattern area and residual layer (Figure 2a), where particles on the residual layer (wider stripes) are highlighted by dashed circles. The *z*-profile of AFM images confirms that particles about 150−200 nm in diameter cover evenly across the entire film. PVP-treated samples have the lowest number of silver particles on the surface with an average particle size of 413 nm (Figure 2b). The increased particles size is due to the reducing power of PVP[30−32] that results in higher growth rate. Although larger nanoparticles were produced, their locations show no selectivity. On 3-MTS-treated sample, silver particles with an average size of 240 nm are observed (Figure 2c). According to the size and the number of the particles, 3-MTS-treated film also shows higher reducing powder than the control sample, although the reducing power of 3-MTS is lower than that of PVP. Silver particles preferentially appear on the thick pattern area rather than on the thin residual layer. The selectivity of growth is also confirmed by comparing the surface roughness derived by AFM on pattern area and residual layer of three samples (Figure 2d). The average roughness of the pattern area and the residual layer on both control and PVP-treated samples are similar, which shows no selectivity. In comparison, the average roughness of the pattern area on 3-MTS sample is three times higher than that of the residual layer, which indicates the particles predominately appear on the thicker area of the films. When comparing the particle numbers

dx.doi.org/10.1021/am401947r | ACS Appl. Mater. Interfaces 2013, 5, 5423−5429

on both areas, Table 1 reveals that the selective growth ratio (particle number ratio) between pattern area and residual layer

Table 1. Distribution of Silver Particles on the Surface of Silica Patterned Film Synthesized by Heat-Treatment at 160 °C

samples	linear density on pattern area ($1/\mu m$)	selective growth ratio (pattern area/ residual area)
control	0.38	1.22:1
PVP	0.33	2.21:1
3-MTS	0.89	12.92:1

significantly increases from 1.22 and 2.21 on both control and PVP-treated samples to 12.92 on 3-MTS-treated samples. These results were also confirmed by SEM images (Figure 3), where particles on the residual layer (wider stripes) are highlighted by dashed circles, indicating the effect of 3-MTS on selective growth of silver particles.

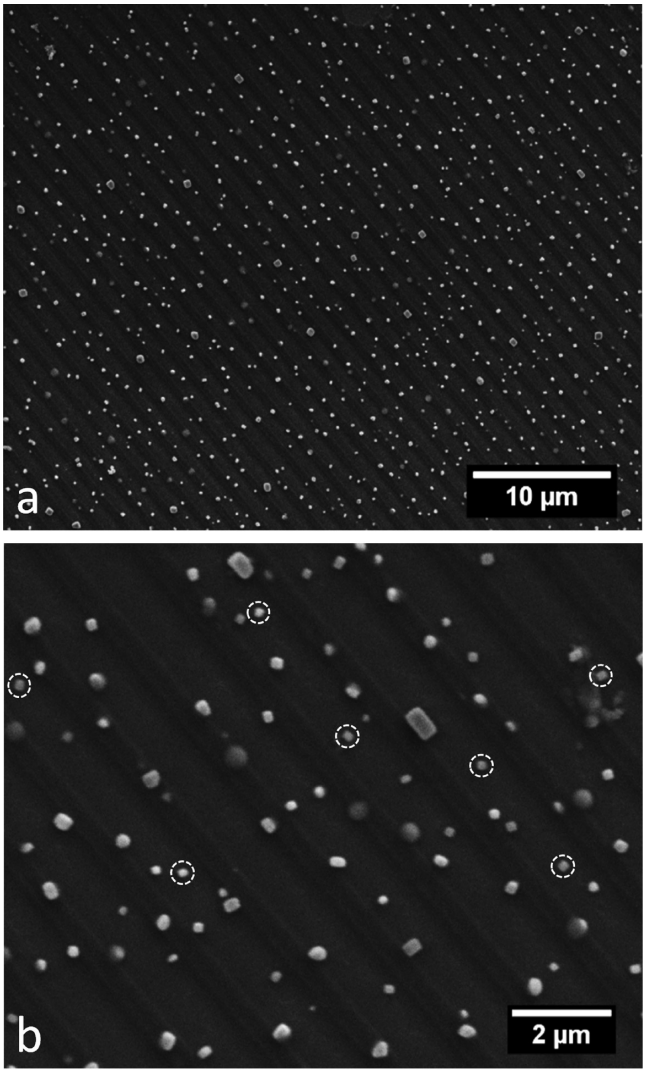

Figure 3. SEM images of patterned silver nanoparticles after heat-treating a silica film containing 3-MTS at 160 °C for 3 h. Images are shown at (a) 2500× and (b) 9000× magnification where particles on the residual layer are highlighted by dashed circles. Silver particles preferentially appear at the pattern area rather than the residual layer of the patterned films, which is consistent with AFM images.

According to previous studies,[25,26] polymer containing silver ions inside the sol–gel derived thin film tends to diffuse to the surface during drying and annealing processes. The driving force is shrinkage-induced stress of the film, which is proportional to film thickness.[33] During heat treatment, PEG oxidizes and reduces silver ions to silver particles at 160 °C.[34,35] This reducing powder depends on the heating temperature and molecular weight of PEG. Therefore, the control sample containing PEG only shows growth of silver particle without selectivity on the location. Although both PVP[30,31] and 3-MTS[36,37] are known to bind to silver ions, PVP tends to diffuse to the surface along with PEG solution during annealing. Hence, silver particles were produced at random locations on the surface. The proposed mechanism behind the selectivity on 3-MTS-treated samples is explained in Scheme 1. First, the silanol group of 3-MTS forms covalent bonds with the silanol group on the silica matrix. Second, shrinkage-induced stress increases with the film thickness.[33] During drying, 3-MTS molecules act as energy barrier to the diffusion motion of silver ions within the matrix. Therefore, most of the silver ions in the thin residual layer (~25 nm thick) are immobilized within the matrix, while on the pattern area (~100 nm thick) more silver ions diffuse to the surface due to higher shrinkage stress and grow into stable crystals during the annealing process. The selectivity may be further increased by increasing the thickness difference between these two areas.

To further examine the selectivity, the same 3-MTS-treated sample was heat-treated at 160 °C for 3 h in a PEG solution containing 1 M $AgNO_3$. SEM images of the resulting surface show that the density of silver crystals on the pattern area has increased (Figure 4) while the density on the residual layer remains constant. Although each stripe pattern about ~1 μm wide consists of individual silver particles aggregates, all newly grown silver particles only appear on the pattern area. Thus, 3-MTS effectively limits the growth of silver only on the thick pattern area regardless of the presence of thin residual layer, which was confirmed to be ~25 nm by AFM. In general, the thickness of residual layer left by the nanoimprint method is about 10–30 nm.[38,39]

To study how temperature affects the selective growth of silver particles, newly prepared 3-MTS-treated films were heat-treated between 400 and 600 °C. SEM images show that the formation of silver nanoparticles begin to appear on the film after 400 °C treatments (Figure 5a). The silver nanoparticles on the pattern area are about ~102 ± 43 nm in diameter with a linear density of 3.36 μm^{-1}. Comparing to the results of low temperature treatment at 160 °C, the linear density of nanoparticles increases ~4 times while the selective growth ratio decreases slightly from 12.92 to 10.32 (Table 2). There are two reasons. First, nucleation rate of nanoparticles is enhanced at high temperature because of higher reduction kinetics. Second, decomposition of PEG at elevated temperature decreases the mobility of silver nanoparticles inside the film and thus limits the growth rate and the size of particles. Thus, silver particles tend to be small at 400 °C instead of forming large particles. After annealing at 600 °C, growth of silver nanoparticles is via Ostwald ripening, where their average size increases to 128 ± 64 nm with a lower linear density of 2.63 μm^{-1} (Figure 5b). The histogram analysis (Figure 5, insets) shows that the dominating particle size increases while the number of particles decreases, confirming the occurrence of Ostwald ripening. These results suggest that the size and

Scheme 1. Selective Growth of Silver Nanoparticles on 3-MTS-Treated Samples[a]

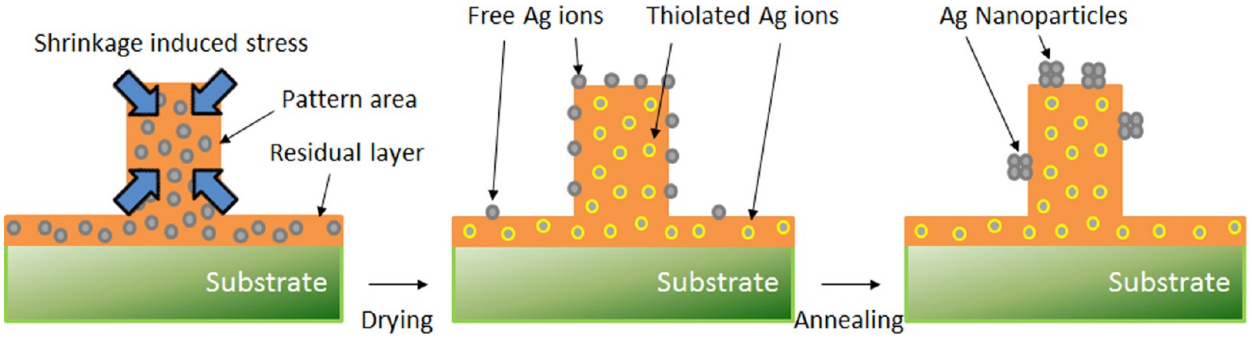

[a]During drying, some Ag^+ ions are trapped by 3-MTS and the remaining Ag^+ ions migrate to the surface along with PEG due to the shrinkage-induced stress. On the pattern area where shrinkage-induced stress is higher, larger number of silver ions migrate to the pattern area with PEG while most of the Ag^+ ions in the residual layer are trapped within the matrix. During annealing, silver ions at the pattern area grow into stable crystals.

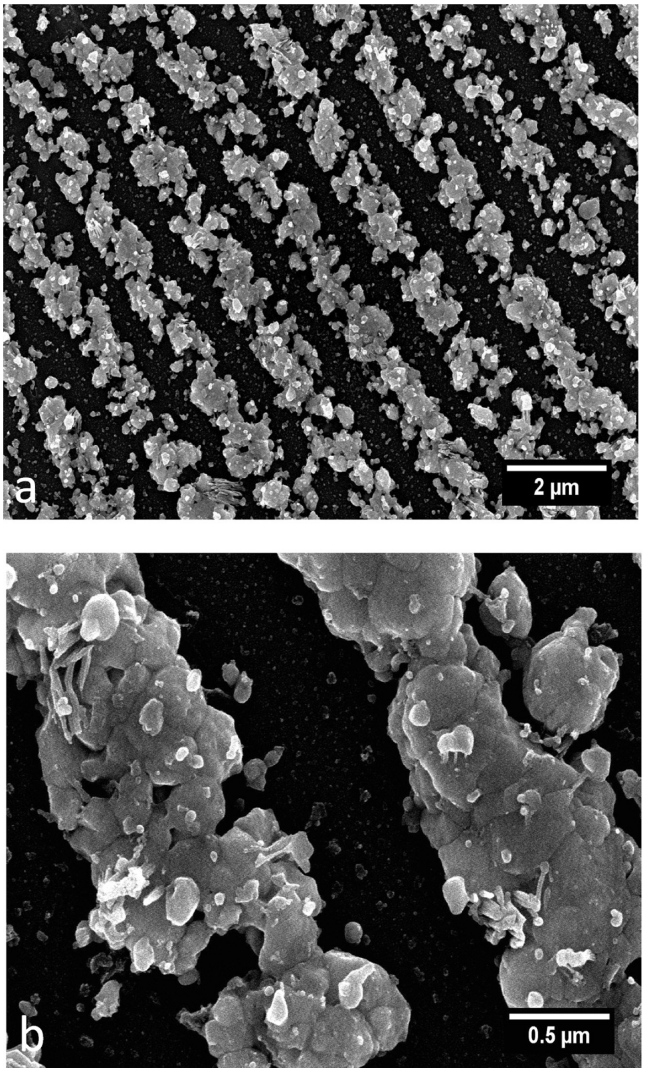

Figure 4. High density of silver crystals on pattern area is achieved by heat-treating a silica film containing 3-MTS at 160 °C for 3 h in a PEG solution containing 1 M $AgNO_3$. The density of silver crystals on the pattern area increases while the density on residual layer remains constant. The images are shown at (1) 9000× and (2) 40 000×.

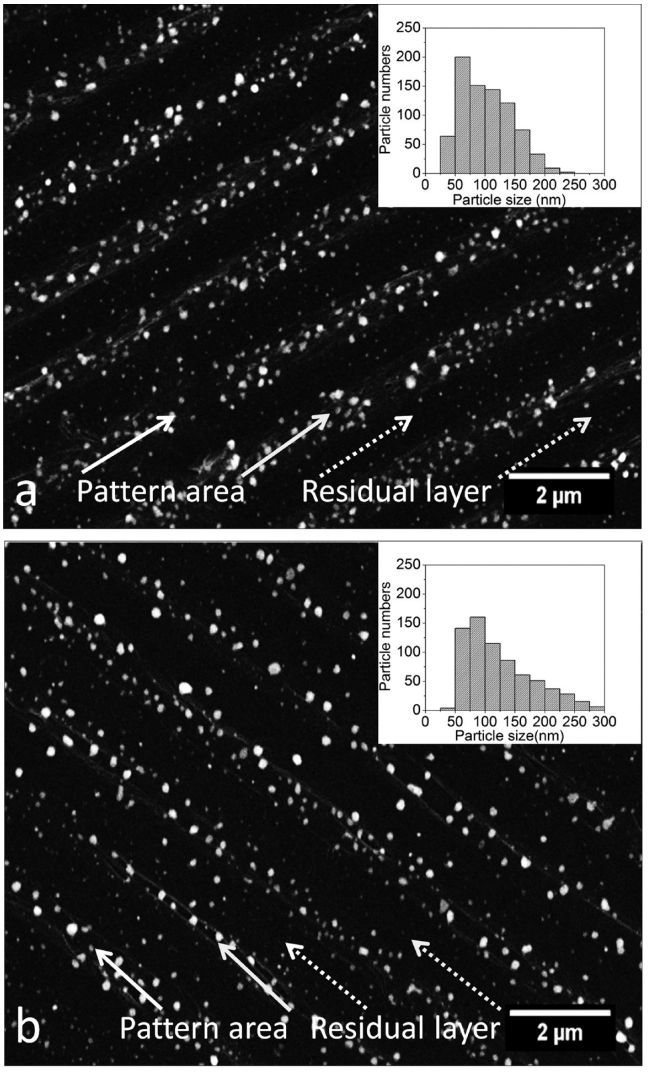

Figure 5. SEM images of patterned silver nanoparticles created by heat-treating silica film containing 3-MTS for 90 min at (a) 400 °C and (b) 600 °C. It shows the average size of silver particles increases with temperature. However, the histogram analysis (inset) shows that the dominating particle size increases while the number of particles decreases after 600 °C treatment.

density of silver nanoparticles can be controlled by the treatment temperature.

Although high temperature treatment enhances the silver reduction reaction, it also reduces the selectivity. To improve

dx.doi.org/10.1021/am401947r | ACS Appl. Mater. Interfaces 2013, 5, 5423−5429

Table 2. Distribution of Silver Particles on the Surface of Silica Patterned Film Synthesized by Heat-Treatment at 400−600 °C and ELD

treatment	linear density on pattern area ($1/\mu m$)	selective growth ratio (pattern area/residual area)
400 °C	3.36	10.32:1
600 °C	2.63	9.86:1
ELD	5.65	20.31:1

the selectivity, we also explored an alternative room temperature process (method 2). This is achieved by growing a layer of metal nanoparticles directly at the surface using a procedure similar to the electroless deposition (ELD). ELD is a low-cost method for creating a variety of metals or alloys coating on nonconductive substrates.[40] This method uses highly reductive diamminesilver(I) complex created from silver nitrate and ammonium. Known as Tollens reagent,[41−44] diamminesilver(I) complex is commonly used to oxidize aldehyde to carboxylic acid, while at the same time ionic silver is reduced to elemental silver. Here, an ammonium hydroxide solution with silver complex ions was utilized to treat samples. Figure 6a is the SEM image of silver nanoparticles produced on the silica film containing ammonium hydroxide and 3-MTS (solution 2) after treating in silver nitrate solution at room temperature for 20 h. The nanoparticles preferentially appear on the pattern area, indicating the selective growth is still observed. The nanoparticles have an average size of 67 ± 19 nm with a linear density of 5.65 μm^{-1}, which is comparable to the density of nanoparticle arrays that exhibit polarization-sensitive optical properties.[45] The histogram of particle size in the Figure 6a inset shows that the normal distribution with the maximum peak is between 60 and 75 nm. On the sample without 3-MTS, nanoparticles unselectively appear on both pattern area and residual layer (Figure 6b). The EDX spectrum confirms the presence of silver nanoparticles on the surface after ELD treatment (Figure 7a). In addition, UV−vis spectroscopy of silver nanoparticles on the patterns reveals a maximum absorption peak at 454 nm (Figure 7b), which corresponds to silver nanoparticles of 65 nm in diameter.[46] In contrast, the sample without ammonium hydroxide shows no absorption peak, indicating no silver nanoparticles are present (Figure 7b).

In the case of PEG, because of its weak reducing power, PEG should be beneficial as a mild and controllable reducing agent. After removing the CD-ROM template, drying-induced stress causes PEG and ammonia to diffuse to the film surface. When soaking the silica film into silver ions solution, the ammonia at the surface of porous silica reacts with silver ions and form diamminesilver(I) complex, which is then reduced to silver by PEG. Due to higher shrinkage stress on the thicker pattern area, larger amount of diamminesilver(I) complex on the surface is expected. At the same time, the stabilized nuclei and crystals are immobilized by the thiol group of 3-MTS on the surface instead of drifting away in the solution. Compared with the sample containing 3-MTS exhibiting selective growth ratio of 20.31:1 (pattern area vs residual layer), the sample without 3-MTS shows more randomly distributed particles, resulting in a selective growth ratio of 1.04:1, about ∼20 times lower. Furthermore, the combination of ammonium and 3-MTS has overall contributed ∼2 times better selectivity of nanoparticle growth at room temperature than the experiment carried out at high temperature (Table 2). Although the ELD process is slow, both higher selectivity and uniform distribution do provide better justification for this procedure. The ELD method also suggests the possibility to selectively grow various metal and alloy nanoparticles with controllable shapes and dimensions on patterns at mild conditions.

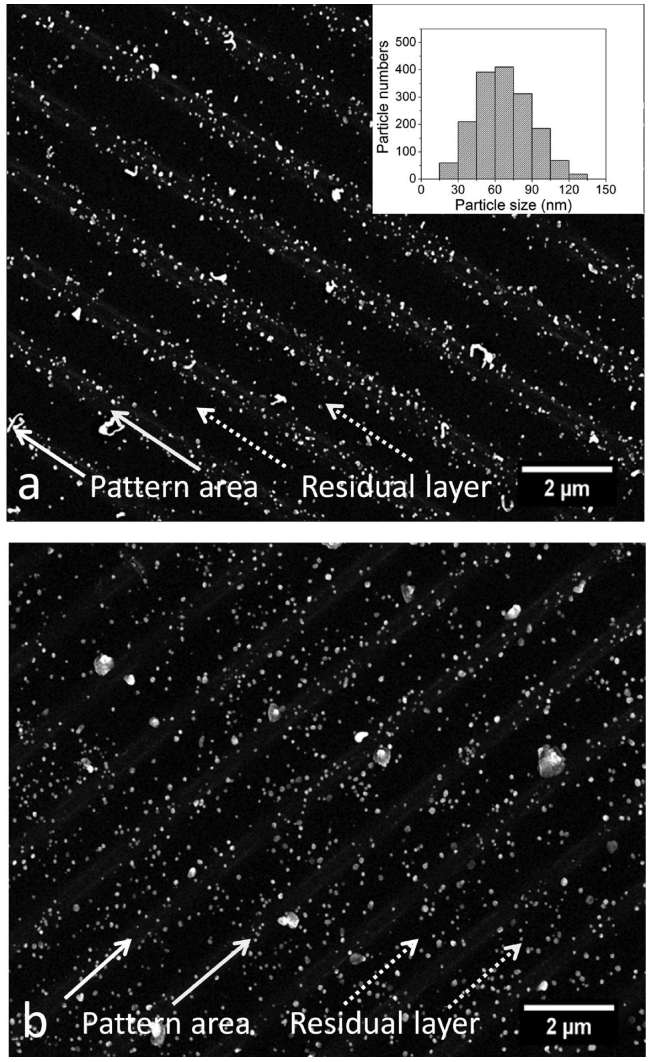

Figure 6. SEM images of patterned silver nanoparticles that were produced by treating silica films made of PEG-sol and ammonium hydroxide (a) with and (b) without 3-MTS in 1 M $AgNO_3$ solution at room temperature for 20 h. The nanoparticles preferentially appear at the thicker pattern area on the samples with 3-MTS, whereas nanoparticles appear evenly on both pattern area and residual layer on the sample without 3-MTS.

4. CONCLUSIONS

A simple but effective method has been utilized to produce silver nanoparticles on silica film patterns created by nanoimprint method without removing the residual layer. The selectivity is the result of 3-MTS additives and films thickness (∼100 nm) that form higher energy barrier to the mobility of Ag ions and crystal nucleation size. The average size of silver nanoparticles on the pattern can be controlled between 100−120 nm by heat treatment. Similarly, silver nanoparticles of 67 nm in diameter with a linear density of 5.65 μm^{-1} can be produced at room temperature by ELD method. Both methods selectively grew silver nanoparticles with a selective growth ratio between 10−20 times on thick pattern area vs thin residual layer (∼25 nm). This method can be easily adapted to

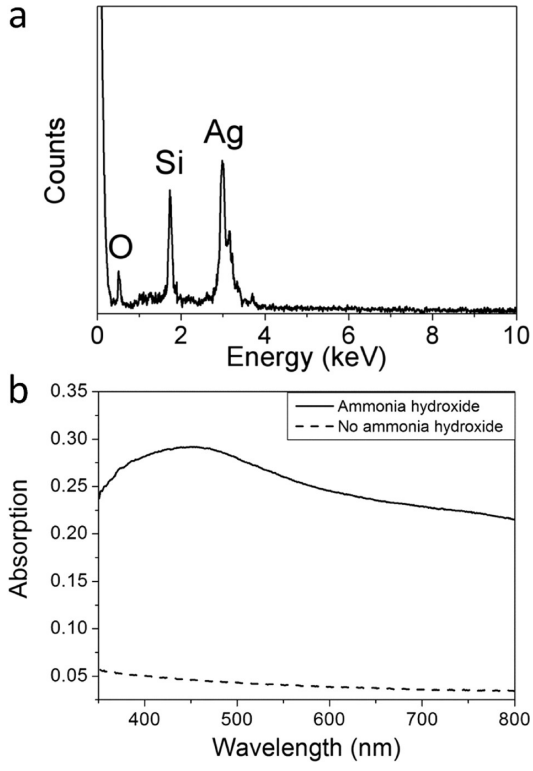

Figure 7. (a) EDX spectrum of ELD treated silica film indicates the presence of silver nanoparticles. (b) UV−vis spectrum of two silica films, one with ammonium hydroxide (solid line) and one without (dashed line), show different silver absorption after treated in 1 M $AgNO_3$ solution at 25 °C for 20 h.

pattern nanoparticles of metal, metal oxide, and semiconductor materials.

AUTHOR INFORMATION

Corresponding Author

*E-mail: cchiu3@ncsu.edu.

Notes

The authors declare no competing financial interest.

REFERENCES

(1) Hutter, E.; Fendler, J. H. *Adv. Mater.* **2004**, *16*, 1685−1706.
(2) McConnell, W. P.; Novak, J. P.; Brousseau, L. C.; Fuierer, R. R.; Tenent, R. C.; Feldheim, D. L. *J. Phys. Chem. B* **2000**, *104*, 8925−8930.
(3) Feldheim, D. L.; Keating, C. D. *Chem. Soc. Rev.* **1998**, *27*, 1−12.
(4) Schmid, G.; Simon, U. *Chem. Commun.* **2005**, 697−710.
(5) Haes, A. J.; Van Duyne, R. P. *J. Am. Chem. Soc.* **2002**, *124*, 10596−10604.
(6) Nam, J. M.; Thaxton, C. S.; Mirkin, C. A. *Science* **2003**, *301*, 1884−1886.
(7) Shipway, A. N.; Katz, E.; Willner, I. *ChemPhysChem* **2000**, *1*, 18−52.
(8) Quinten, M.; Leitner, A.; Krenn, J. R.; Aussenegg, F. R. *Opt. Lett.* **1998**, *23*, 1331−1333.
(9) Pinchuk, A. O.; Schatz, G. C. *Mater. Sci. Eng., B* **2008**, *149*, 251−258.
(10) Riboh, J. C.; Haes, A. J.; McFarland, A. D.; Yonzon, C. R.; Van Duyne, R. P. *J. Phys. Chem. B* **2003**, *107*, 1772−1780.
(11) Mendes, P. M.; Jacke, S.; Critchley, K.; Plaza, J.; Chen, Y.; Nikitin, K.; Palmer, R. E.; Preece, J. A.; Evans, S. D.; Fitzmaurice, D. *Langmuir* **2004**, *20*, 3766−3768.
(12) Kuznetsov, A. I.; Evlyukhin, A. B.; Goncalves, M. R.; Reinhardt, C.; Koroleva, A.; Arnedillo, M. L.; Kiyan, R.; Marti, O.; Chichkov, B. N. *ACS Nano* **2011**, *5*, 4843−4849.
(13) Spatz, J. P.; Mossmer, S.; Hartmann, C.; Moller, M.; Herzog, T.; Krieger, M.; Boyen, H. G.; Ziemann, P.; Kabius, B. *Langmuir* **2000**, *16*, 407−415.
(14) Kastle, G.; Boyen, H. G.; Weigl, F.; Lengl, G.; Herzog, T.; Ziemann, P.; Riethmuller, S.; Mayer, O.; Hartmann, C.; Spatz, J. P.; Moller, M.; Ozawa, M.; Banhart, F.; Garnier, M. G.; Oelhafen, P. *Adv. Funct. Mater.* **2003**, *13*, 853−861.
(15) Maury, P.; Escalante, M.; Reinhoudt, D. N.; Huskens, J. *Adv. Mater.* **2005**, *17*, 2718−2723.
(16) Kinge, S.; Crego-Calama, M.; Reinhoudt, D. N. *ChemPhysChem* **2008**, *9*, 20−42.
(17) Ko, S. H.; Park, I.; Pan, H.; Grigoropoulos, C. P.; Pisano, A. P.; Luscombe, C. K.; Frechet, J. M. J. *Nano Lett.* **2007**, *7*, 1869−1877.
(18) Martensson, T.; Carlberg, P.; Borgstrom, M.; Montelius, L.; Seifert, W.; Samuelson, L. *Nano Lett.* **2004**, *4*, 699−702.
(19) Zhao, W.; Low, H. Y.; Suresh, P. S. *Langmuir* **2006**, *22*, 5520−5524.
(20) Kao, Y. C.; Hong, F. C. N. *J. Micromech. Microeng.* **2011**, *21*, 1−8.
(21) Park, H.; Cheng, X. *Nanotechnology* **2009**, *20*, 1−7.
(22) Routkevitch, D.; Bigioni, T.; Moskovits, M.; Xu, J. M. *J. Phys. Chem.* **1996**, *100*, 14037−14047.
(23) Feng, S.; Bein, T. *Nature* **1994**, *368*, 834−836.
(24) Chen, C. C.; Lin, J. J. *Adv. Mater.* **2001**, *13*, 136−139.
(25) Chiu, C. K.; Choi, Y. J.; Luo, T. J. M. *Cryst. Growth Des.* **2012**, *12*, 4727−4732.
(26) Chen, T. Y.; Chiu, C. K.; Choi, Y. J.; Luo, T. J. M.; Lin, T. L. *J. Mater. Sci.* **2013**, *48*, 850−856.
(27) Laibinis, P. E.; Whitesides, G. M.; Allara, D. L.; Tao, Y. T.; Parikh, A. N.; Nuzzo, R. G. *J. Am. Chem. Soc.* **1991**, *113*, 7152−7167.
(28) Schreiber, F. *Prog. Surf. Sci.* **2000**, *65*, 151−256.
(29) Sellers, H.; Ulman, A.; Shnidman, Y.; Eilers, J. E. *J. Am. Chem. Soc.* **1993**, *115*, 9389−9401.
(30) Washio, I.; Xiong, Y. J.; Yin, Y. D.; Xia, Y. N. *Adv. Mater.* **2006**, *18*, 1745−1749.
(31) Huang, H. H.; Ni, X. P.; Loy, G. L.; Chew, C. H.; Tan, K. L.; Loh, F. C.; Deng, J. F.; Xu, G. Q. *Langmuir* **1996**, *12*, 909−912.
(32) Sun, Y. G.; Mayers, B.; Herricks, T.; Xia, Y. N. *Nano Lett.* **2003**, *3*, 955−960.
(33) Hench, L. L.; West, J. K. *Chem. Rev.* **1990**, *90*, 33−72.
(34) Luo, C. C.; Zhang, Y. H.; Zeng, X. W.; Zeng, Y. W.; Wang, Y. G. *J. Colloid Interface Sci.* **2005**, *288*, 444−448.
(35) Nam, S.; Parikh, D. V.; Condon, B. D.; Zhao, Q.; Yoshioka-Tarver, M. *J. Nanopart. Res.* **2011**, *13*, 3755−3764.
(36) Shankaran, D. R.; Uehera, N.; Kato, T. *Sens. Actuators, B* **2002**, *87*, 442−447.
(37) Guo, H. Q.; Tao, S. Q. *Sens. Actuators, B* **2007**, *123*, 578−582.
(38) Lee, H. J.; Ro, H. W.; Soles, C. L.; Jones, R. L.; Lin, E. K.; Wu, W. L.; Hines, D. R. *J. Vac. Sci. Technol. B* **2005**, *23*, 3023−3027.
(39) Kim, K. D.; Jeong, J. H.; Sim, Y. S.; Lee, E. S. *Microelectron. Eng.* **2006**, *83*, 847−850.
(40) Paunovic, M.; Schlesinger, M. *Fundamentals of Electrochemical Deposition*; John Wiley & Sons: New York, 1998.
(41) Yin, Y. D.; Li, Z. Y.; Zhong, Z. Y.; Gates, B.; Xia, Y. N.; Venkateswaran, S. *J. Mater. Chem.* **2002**, *12*, 522−527.
(42) Montazer, M.; Alimohammadi, F.; Shamei, A.; Rahimi, M. K. *Carbohydr. Polym.* **2012**, *87*, 1706−1712.
(43) Benet, W. E.; Lewis, G. S.; Yang, L. Z.; Hughes, D. E. P. *J. Chem. Res* **2011**, 675−677.
(44) Dondi, R.; Su, W.; Griffith, G. A.; Clark, G.; Burley, G. A. *Small* **2012**, *8*, 770−776.
(45) Zdyrko, B.; Kinnan, M. K.; Chumanov, G.; Luzinov, I. *Chem. Commun.* **2008**, 1284−1286.
(46) Bogle, K. A.; Dhole, S. D.; Bhoraskar, V. N. *Nanotechnology* **2006**, *17*, 3204−3208.